



Original Article

Effect of electropulsing on the solidification of mould flux



Ashutosh G. Bhagurkar, Rongshan Qin^{*}

School of Engineering and Innovation, The Open University, Walton Hall, Milton Keynes, MK7 6AA, United Kingdom

ARTICLE INFO

Article history:

Received 25 March 2022

Accepted 31 May 2022

Available online 4 June 2022

Keywords:

Electropulsing

Mould flux

Solidification

Microstructure

ABSTRACT

The effect of electropulsing on the microstructure formation in solidification of mould flux has been investigated. Experimental characterization and image analysis reveals that the electropulsing treatment reduces 46% porosity and increases the interfacial perimeter to area ratio by 100%. The latter provides strong evidence that electric current influences interfacial energy. Dendrite arm spacing is reduced considerable. Electropulsing promotes the anisotropic crystal growth and retards the formation of interconnected crystal network. The latter is favourable to the current flow, liquid refilling and lubrication. The work demonstrates that electropulsing can be used to modify the microstructure of slag and hence to control the horizontal heat transfer rate in the mould, which is desirable in continuous casting of advanced high strength steels.

© 2022 The Author(s). Published by Elsevier B.V. This is an open access article under the CC BY license (<http://creativecommons.org/licenses/by/4.0/>).

1. Introduction

A thin film of slag forms from the solidification of molten mould flux in the gap between mould and steel in continuous casting. This film, albeit in a few millimetres thick, plays an important role in managing the horizontal heat transfer from liquid metal to casting mould and providing lubrication for the relative movement between parts [1]. To cast the newly developed advanced high strength steels, e. g. the high manganese or rare earth elements alloyed steels [2,3], the microstructure and properties of slag film are demanded to be modified. This is, however, not easy to achieve by tuning the chemical-thermo-mechanical processing conditions because the chemical constitution of the mould flux have been designed to meet many other requirements such as inclusion absorption and surface reaction on the top of liquid metal and in meniscus, and the thermomechanical processing is unable

to reach the tiny inner gap. Electropulsing treatment is, therefore, explored in the present work to testify its suitability to fulfil the engineering expectations.

The literature about the effect of electropulsing on the solidification is considerably rich [4]. Misra observed the current-induced microstructure refinement in the solidification of metals in 1980s [5–7]. Li et al. observed the current-induced anisotropic crystal growth [8]. Barnak et al. characterized the relationship between grain size and current density in the solidification of Sn–Pb alloys quantitatively [9]. Qin et al. derived an equation to describe the density-dependent grain size in the casts of metals and alloys based on electric current thermodynamics [10]. Zhang et al. found that electropulsing can change the configuration of non-metallic inclusions in liquid metals [11]. Electropulsing treatment has been implemented to many engineering alloys [12–14]. The commonly agreed fundamental understanding includes the electric current enhanced solute mobility [15], alternated

^{*} Corresponding author.

E-mail address: rongshan.qin@open.ac.uk (R. Qin).

<https://doi.org/10.1016/j.jmrt.2022.05.188>

2238-7854/© 2022 The Author(s). Published by Elsevier B.V. This is an open access article under the CC BY license (<http://creativecommons.org/licenses/by/4.0/>).

kinetic barrier for microstructural transformation [16] and added thermodynamic effect [17]. Electropulsing-enhanced mobility has also been observed in solidification of mould flux and sintering of ceramic powders. Riaz reported a glassy to crystal transformation in the solidification of mould flux [18]. The improved mobility enables the formation of tiny crystals after diffusion before being frozen to amorphous state. The lower-than-expected sintering temperature in plasma processing of ceramic powder is also attributed to the enhanced mobility [19]. The reduced kinetic barrier and enhanced mobility shares a common mechanism with the well-established electroplasticity [20,21].

However, the understanding of the effect of electropulsing on the microstructural evolution in solidification is still far from satisfactory. One of the most important questions is whether electropulsing affects solid–liquid interfacial energy. In the work reported by Barnak et al. [9], electropulsing was suggested to influence the solid–liquid interfacial energy. The suggestion was made to explain the current-affected nucleation rate without further evidence. In the homogeneous nucleation theory, the critical radius (r_c) for a nucleus to grow rather than to shrink is expressed as

$$r_c = 2\sigma_{LS}/g_{LS} \quad (1)$$

where σ_{LS} and g_{LS} are the interfacial energy and free energy density difference between liquid and solid phases, respectively. Eq. (1) shows that a smaller interfacial energy corresponds to a smaller critical radius. The nucleation rate (n_c) to form crystal nuclei above the critical radius is expressed as

$$n_c = n_0 \exp\left(-\frac{16\pi\sigma_{LS}^3}{3KTg_{LS}^2}\right) \quad (2)$$

where n_0 is the total number of atoms in the system, K the Boltzmann constant and T the temperature. Eq. (2) shows that a smaller interfacial energy corresponds to a higher nucleation rate. However, interfacial energy is not the only factor to influence the critical radius of crystal nuclei. The additional electrical current free energy g_{LS}^E possesses the similar effect when $g_{LS}^E > 0$

$$g_{LS} = g_{LS}^O + g_{LS}^E \quad (3)$$

This means that the further evidence other than the electropulsing improved the nucleation rate is required to clarify the electropulsing-affected solid–liquid interfacial energy. This challenge has been addressed in the present work by consideration of crystal growth and microstructural formation. Interface energy and configuration of microstructure has a strong influence on the formation and of porosity in the solidification. Pores are formed by two mechanisms. One is due to volume shrink during temperature dropping in the solidification. Liquid is unable to fill the gaps that are formed by the volume shrink due to the blocked flowing channel by the

interconnected crystals and the increased apparent viscosity [22]. Another is due to the gas bubbles being trapped between the crystals. In analogy to the electropulsing-driven inclusion removal [11] and hydrogen mitigation [23], electropulsing should possess the similar effect to improve the situation. This problem has also been investigated in the present work. The modified porosity contributes to many properties in the slag film [24]. The work is organized as the followings. Section 2 describes the experimental setup and procedures. The results are presented in section 3. Section 4 provides discussion toward scientific understanding of the observations, which is followed by inclusions and remarks in section 5.

2. Experiments

The mould powders were received from a project partner at Sandvik AB in Sweden. The chemical composition of the as-received materials is listed at the second row (noted as Recv.) in Table 1, where others represent the combination of H_2O , C, biocarbonates and organic matters. The physical properties of the as-received powders are: softening temperature 1333 K, melting temperature 1423 K, flowing temperature 1433 K and density 570 kg/m³.

The powders were heated to 1173 K and maintained for 4 hours to remove H_2O , carbonaceous and other volatile constitutions. The heat-treated powders were melted in graphite crucibles by an induction furnace. After the induction heating was turned off, two electrodes made by pure iron were inserted to the molten mould flux. The electrodes are iron rods with rectangular cross-section of 8 mm × 6 mm. The distance between the electrodes is about 12 mm from edge to edge. Those electrodes can be removed easily from the solidified mould flux due to low wettability between them. A thermocouple was inserted to the liquid with the tip located in the central area between electrodes. The molten mould flux was allowed to air cooling in the ambient conditions. The solidification was performed in two groups. Both groups have the electrode inserted in the liquid but only the pulsated samples had the electrodes connected to an electric current pulse generator. The electropulsing were with a peak current density 2×10^4 A/m², each pulse's duration at 60 μ s and a pulse frequency at 500 Hz. The reference samples had the electropulsing generator disconnected to the electrodes. The setting enabled both the reference and pulsated samples to experience the identical thermal history. This leaves the electropulsing to be the only distinguishable factor. The experimental set-up is schematically illustrated in Fig. 1. The electric current pulses were generated by AVTECH (AV-108F-2-B-P) that was powered by Delta Elektronika (SM1500 series). The solidified samples were cut along the longitudinal section, polished and examined by optical microscope, scanning electron microscopy (SEM) with energy dispersive spectroscopy (EDS) using Zeiss Supra 55 VP FEG SEM.

Table 1 – The chemical composition of the as-received and modified mould powders (wt.%).

	CaO	SiO ₂	Na ₂ O	Al ₂ O ₃	F	MnO	Fe ₂ O ₃	MgO	TiO ₂	K ₂ O	Others
Recv.	27.82	19.87	7.64	7.51	6.56	5.9	0.96	0.79	0.31	0.14	22.50
Modi.	33.60	24.00	9.23	9.07	7.92	7.13	1.16	0.95	0.37	0.17	6.4

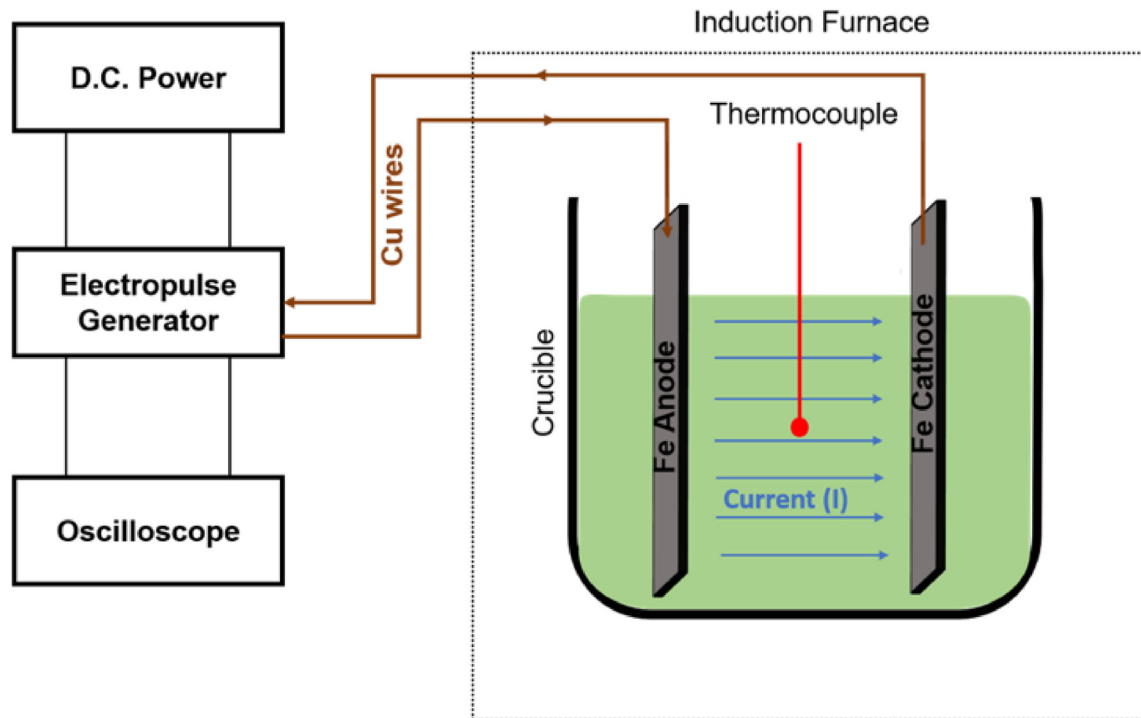


Fig. 1 – Schematic diagram for the experimental setup. Electropulsing was disconnected for the reference samples.

The microstructures at several positions from anode to cathode have been examined.

Thermogravimetric analysis (TGA) was used to measure the weight loss/gain in the sample during the heat treatment. The measurements were performed in Ar gas (99.9% purity) atmosphere with a flow rate of 10^{-6} m³/s. Platinum was used as reference material. Approximately 0.06 g of as-received powders were heated at a constant heating rate of 20 K/min from room temperature to 1523 K in a platinum crucible with a diameter of 5 mm and a height of 5 mm.

3. Results

Figure 2 shows the TGA measurement during the heating up of the as-received mould flux from room temperature to 1523 K. The total weight loss is 17.2%. The endothermic peaks correspond to water evaporation and carbonaceous substance giving away CO₂, while exothermic peak indicates graphite combustion. The chemical constitutions have been recalculated according to the measurement, and the results are listed in the third row in Table 1. It is worth to point out that many literatures describe the chemical constituents of mould flux in less than a total 100% because of the weight loss during the heating up, as has been summarized recently in literature [25].

The microstructures for the reference (left column) and pulsated samples (right column) are shown in Fig. 3. Three representative positions from anode to the centre between two electrodes are presented. The images at the top row are from the position adjacent to the anode. Insertion of electrodes produces chilling effect and disturbance to this position. Some columnar grains from directional solidification can be seen

from Fig. 3(a), showing the chilling effect and reflecting the temperature gradient. The direction of electric field gradient is indicated by an arrow. The temperature gradient is in the parallel direction. The bottom row is from the position at the centre between two electrodes and hence least affected by the insertion of electrodes. No temperature gradient can be seen from Fig. 3(e). The middle row images are from the position between them. Fig. 3 indicates, therefore, the effect of electropulsing on the solidification at various cooling rates and mechanical disturbances. Two obvious differences have been noted from the microstructures formed without and with electropulsing treatment. The first is that the fraction of porosity in the pulsated samples (the images in the right column) is much smaller than that in the reference samples (the images in the left column). The pores appear as dark holes in those images. Image J analysis revealed that the microstructure in reference sample consists of 6.5% mean porosity while that in pulsated sample has 3.5% only. Electropulsing treatment reduces over 46% of the average porosity. The second is that the amount of interface between the bright (primary crystals) and dark background (matrix) is significantly increased by the electropulsing treatment. Image J analysis shows that average interfacial perimeter to area ratio of the primary crystals has been increased from 0.08 to 0.16 by electropulsing treatment, which is an increment of 100%.

To characterize the primary crystals and the matrix in order to understand the solidification procedure, Fig. 4 shows a back-scatter electron image taken from the reference sample. The primary crystal (bright part) contains one phase, while the dark background contains two phases to form eutectic structure.

EDS map taken on a reference sample shows that the primary crystals contain rich Ca, Si and F, which is a strong

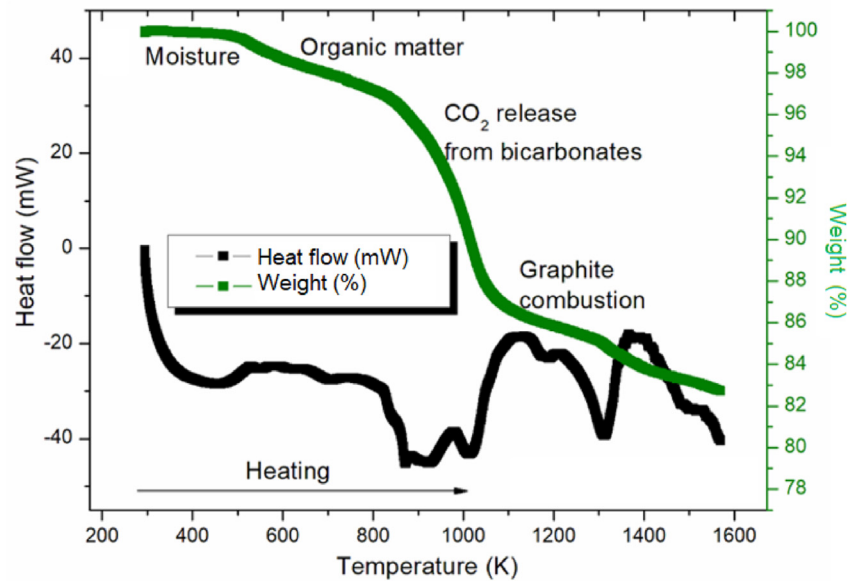


Fig. 2 – TGA measurement shows 17% weight loss and associated heat flow pattern when the as-received mould power is heated up from ambient temperature to 1523 K.

indication of cuspidine ($2\text{SiO}_2 \cdot 3\text{CaO} \cdot \text{CaF}_2$) phase. The background region contains rich Na, Al, Mn and O, showing the presence of nepheline ($\text{NaAlSi}_3\text{O}_8$) and other residual elements. CaF_2 particles are noticed in the dark background areas, as is labelled in circle in Fig. 5. No detectable contaminations either from iron electrode or from graphite crucible was detected in any of the samples. Similar analysis has also been performed to the electropulsing treated samples. There are no noticeable differences in composition distributions between the primary crystals and matrix found. The volume fraction of the primary phase in both the reference and pulsed samples are in a similar value.

During the pulsed solidification experiments, the output current and the temperature have been monitored. The values are plotted in Fig. 6. There are three characteristic temperatures labelled in the figure, corresponding to the beginning of the formation of cuspidine primary crystal at 1423 K, beginning the formation of eutectic structure at 1193 K and the beginning the formation of the final Ca_2F crystal at 890 K. It can be seen from Fig. 6 that the overall electrical conductance of the considered mould flux is much larger than that of the other oxides mixtures. An electric current over 10 A has been observed in a wide range of temperature. The reason for the high electrical conductivity is attributed to the high concentration of fluorine (7.92 wt.%) and high residual carbon (6.4 wt.%). Fluorine forms CaF_2 , which in liquid state is with relative high conductivity according to literature [26]. The electrical conductivity of CaF_2 is $> 4 \Omega^{-1}\text{cm}^{-1}$ and its mixture with CaO and Al_2O_3 are over $3 \Omega^{-1}\text{cm}^{-1}$. While the electrical conductivities of many other oxides are between 0.1 and $0.4 \Omega^{-1}\text{cm}^{-1}$ [27]. The residual carbon also contributes to the high electrical conductivity. During the growth of the primary cuspidine crystals, the electric conductivity of the solid–liquid mixture reduces slowly. Cuspidine crystal has lower electrical conductivity than that of the liquid mould flux. Although the growing of the volume fraction of cuspidine crystal reduces

the system electrical conductance, the percolation effect due to the high connectivity of the residual liquid makes the reduction of the electrical conductance less than the linear one, as is seen in the area between two temperature lines at 1423 K and 1193 K. However, when the eutectic structure begins to grow at 1193 K, the electrical conductance reduces steeply. The observed electric current reduces very quickly in this stage. After the final growth of Ca_2F , almost all the liquid phase solidified, and the materials becomes highly electric resistive. The observed electric current reduces to very low level before disappearing completely.

4. Discussion

An obvious difference between the microstructures in electropulsing treated samples and the reference samples, according to Fig. 3, are the morphology and fraction of the interface. It has been stated that the pulsed samples have the interfacial perimeter to area ratio increased by over 100% in section 3. To demonstrate this more clearly, Fig. 7 shows the distribution of the interface between the primary crystals and the eutectic matrix in (a) part of Fig. 3(e) and (b) part of Fig. 3(f), respectively. The figures have been produced by a functionality in MatVisual software. Many flat interfaces can be found in Fig. 7(a), as that are pointed out by the black arrows. However, the interface in Fig. 7(b) is much more fractal.

The microstructures of electropulsing treated samples possess a number of advantages over that of the reference samples. Firstly, the large pores and high porosity in the reference samples can reduce the strength of the slag film and make the fracture to occur more frequently. The fractured slag film, especially with a large gap or wide crack, can cause the liquid steel to penetrate and stick on the copper mould directly, which is disastrously. Secondly, the distribution of cuspidine phase in electropulsing treated samples is more

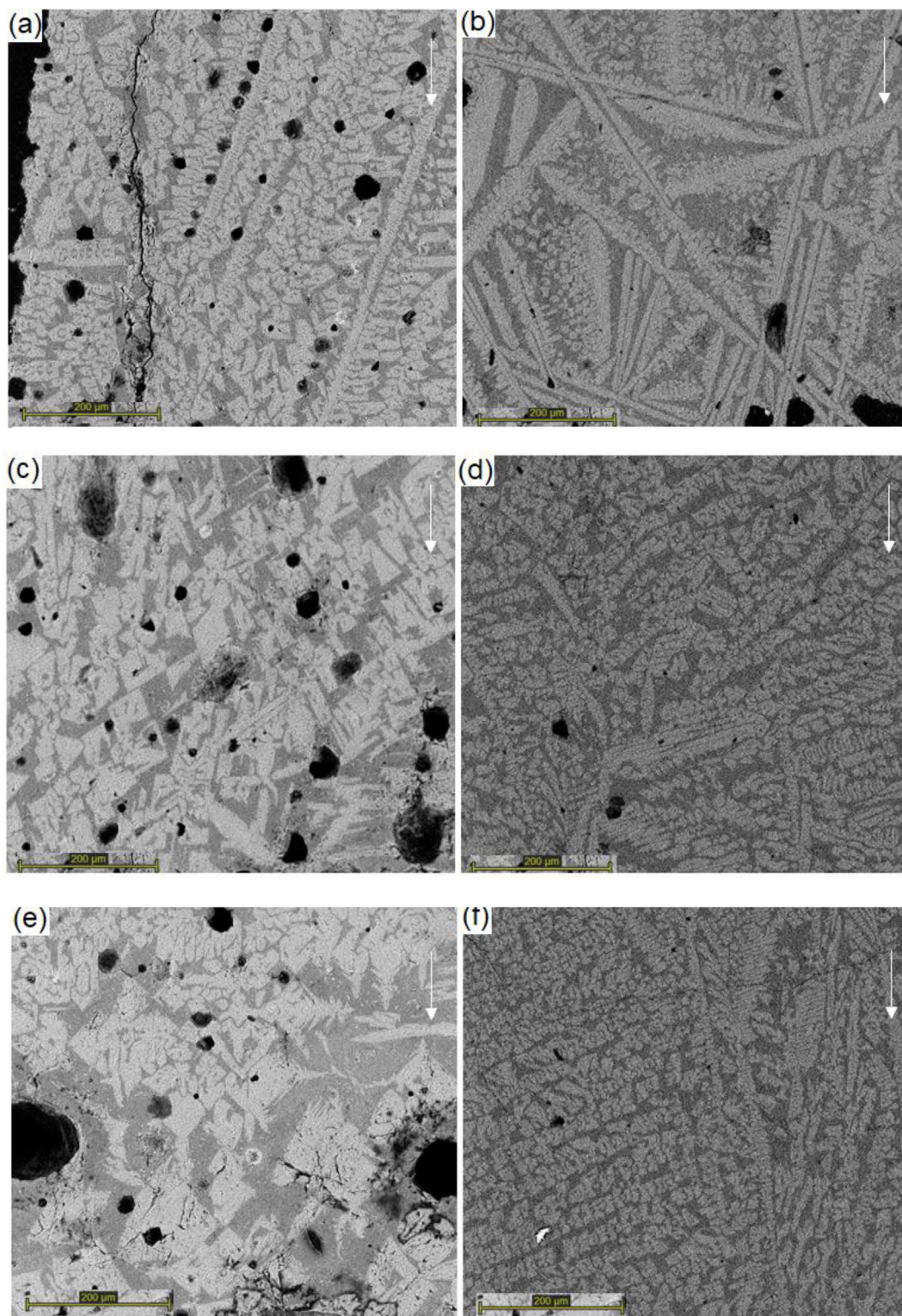


Fig. 3 – The microstructures of reference sample (left column) and electropulsing treated sample (right column). The images at the top row are from the position adjacent to anode, while that in the bottom row are from the middle between two electrode and that in middle row are between them. The arrow in each image represents the direction of electric potential gradient.

homogeneous than that of the reference samples. This can be seen obviously by comparing Fig. 3(f) with Fig. 3(e). Heat transfer is hence more homogeneously in the electropulsing treated samples than that of the reference sample, and the

steel product can have better properties using the electropulsed slag film. Thirdly, the microstructure in the reference samples contains more sharp edges and needle-like crystals than that of the samples treated by electropulsing, as is

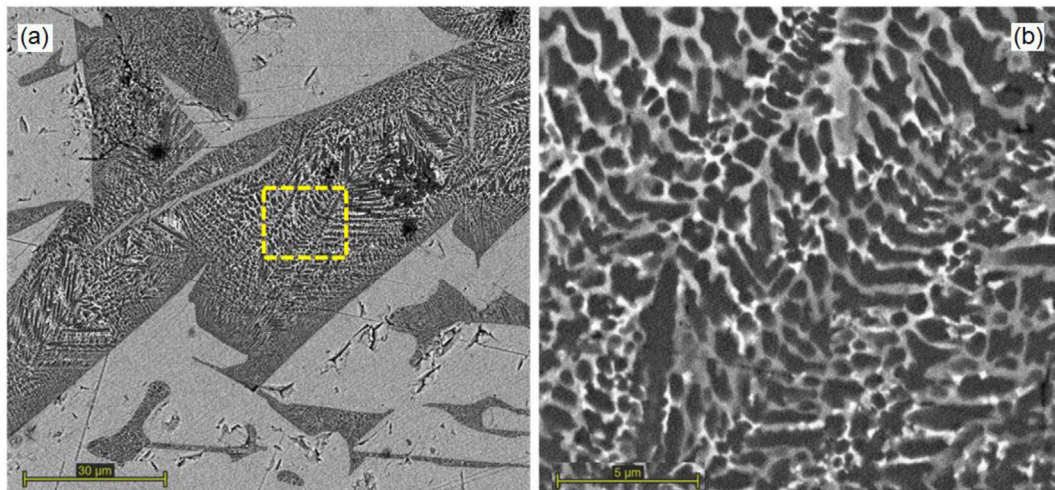


Fig. 4 – (a) Backscatter electron image of reference sample showing bright primary crystals and dark two-phase eutectic structure, where the yellow square is magnified in (b), showing the last solidifying region in the sample.

labelled by the red arrows in Fig. 7(a). The sharp crystal edges are detrimental to the lubrication.

According to the second law of thermodynamics, formation of a microstructure in solidification follows a path to minimize the system free energy. There is no difference for the amount of chemical free energy between the reference and pulsed samples because the volume fraction of the primary crystal in both cases is in similar amount. Although electric current free energy can compensate to some of the increment of interfacial energy in grain refinement [28], the microstructure with smooth interface has been proved to have lower electric current energy than that of the rough interface [29]. This means that the formation of fractal interface cannot be explained by the electric current free energy and the chemical free energy. The only possibility is that the interface energy has been affected by the applied electric field.

To understand the effect of electric treatment on the interface energy, the electric potential distribution in the

solidifying mould flux has been calculated numerically. The detailed calculation has been described and published in another paper [30]. In a brief description, the geometry of a surface of the solidified mould flux was obtained by Leica DCM-3D Profiler. The scanned 3D geometry was input to a logic frame for calculation of electric potential distribution using the realistic electrical conductivities of mould flux. The results are plotted using MatVisual software. Fig. 8 shows the contour of electric potential distribution in the computational logic frame. The dashed line represents an interface. It can be seen that across the interface the electric potential jumps. This indicates an electric potential difference at both sides of the interface. As has been demonstrated in Section 2, mould flux consists of various oxides in relatively poor electrical conductivity. The conductive mechanism is not by electrons but by the moving ionised atoms [31]. The presence of electric potential difference around the interface can cause the oxides to polarize. The rearrangement of the polarized molecules at

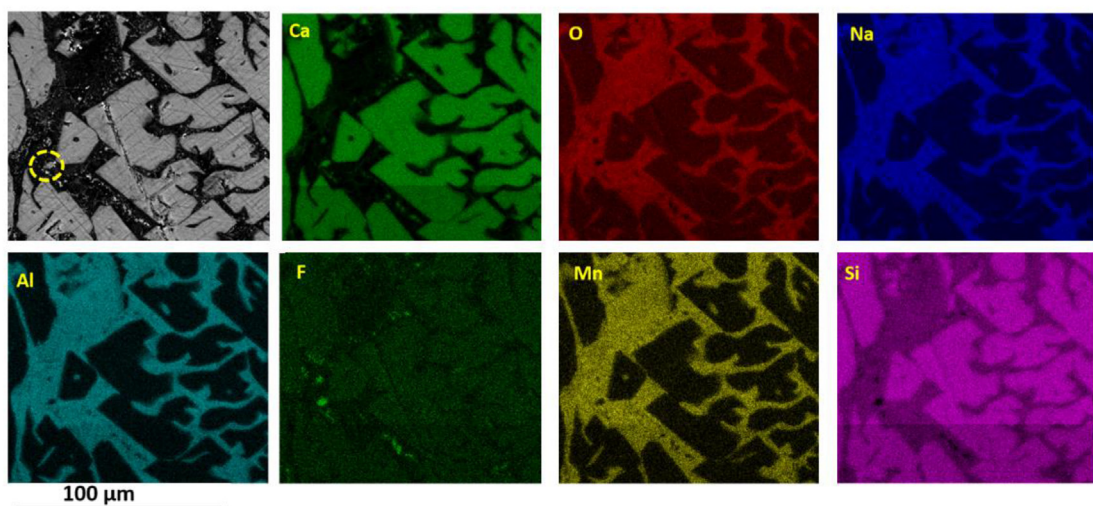


Fig. 5 – EDS map taken on a reference sample showing distribution of constituent elements. The top-left image shows the phase field. The bright regions are rich in Ca, Si and F. The dark background is rich in Na, Al, Mn and O. The yellow circle shows the presence of CaF_2 .

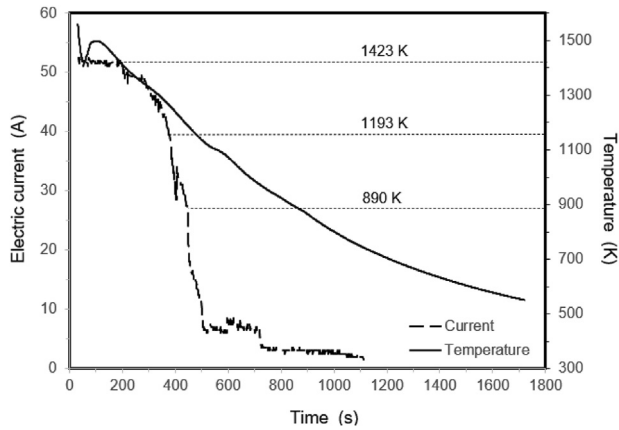


Fig. 6 – Variation of electric current and temperature as function of time in a solidifying mould flux upon application of electropulsing.

interface can reduce the interface energy drastically, sometimes to negative interface energy such as that in surfactant and missile [32]. The reduced interface energy enables the growing of crystals with fractal surface.

According to the Mullins–Sekerka interface instability theory for the crystal growth [33], formation of the fractal solid–liquid interface is controlled by three major factors, namely interfacial energy, temperature distribution and solute diffusivity. This is described by the following kinetic equation [33].

$$S(\omega) = -T_m \sigma_{LS} \omega^2 - (\Theta_{\infty} + \Theta_{\square}) + 2mG_c \frac{[\omega^* - (V/D)]}{[\omega^* - (V/D)p]} \quad (4)$$

where $S(\omega) > 0$ leads to the formation of a fractal interface but $S(\omega) < 0$ indicates a planar interface to grow. ω is the interface fluctuation frequency. In the first term on the right hand of Eq. (4), T_m is the melting temperature and σ_{LS} is the interfacial energy. A larger interfacial energy makes $S(\omega)$ smaller, which

indicates a less fractal or planar interface. In the opposite case, a smaller or even a negative interfacial energy can make $S(\omega) > 0$ or even bigger to grow a more fractal morphology. Θ_{∞} and Θ_{\square} are two parameters dependent on the temperature gradient and thermal conductivities in solid side and liquid side around the interface. According to the calculate to be demonstrated later in this work, electropulsing has negligible effect on the temperature change in the system and hence imposes negligible effect on the second factor of $(\Theta_{\infty} + \Theta_{\square})$. In the third term on the right hand of Eq. (4), m is the slope of the liquidus. G_c is the concentration gradient in the liquid at the unperturbed flat interface. V is the solidification rate. D is the diffusivity. $p = 1 - k$ with k the equilibrium partition ratio. ω^* is defined as

$$\omega^* = \frac{V}{2D} + \sqrt{\left(\frac{V}{2D}\right)^2 + \omega^2} \quad (5)$$

It is well-known that electropulsing enhances solute diffusion [15,29]. The enhanced diffusion reduces concentration gradient and hence reduces the contribution of solute diffusion to the formation of fractal pattern. This trend is in agreement with the famous phenomena reported in diffusion-limited agglomeration [34]. In summary of the above analysis, the electropulsing-induced interfacial energy reduction is the only possibility to explain the observed microstructural evolution.

Fig. 3(a), (c) and (e) reveal that many pores are formed in the matrix areas surrounded by the primary crystals. The interconnected primary crystals block the way for liquid phase to flow and fill those gaps formed by volume shrink during the solidification of the materials. It also blocks the way for the formed gas bubbles to escape. However, the microstructures presented in Fig. 3(b), (d) and (f) show more connected liquid field, which is clearly demonstrated by the curve AB in Fig. 7(b). This promotes the liquid refilling and gas bubble escaping and hence retaining less pores.

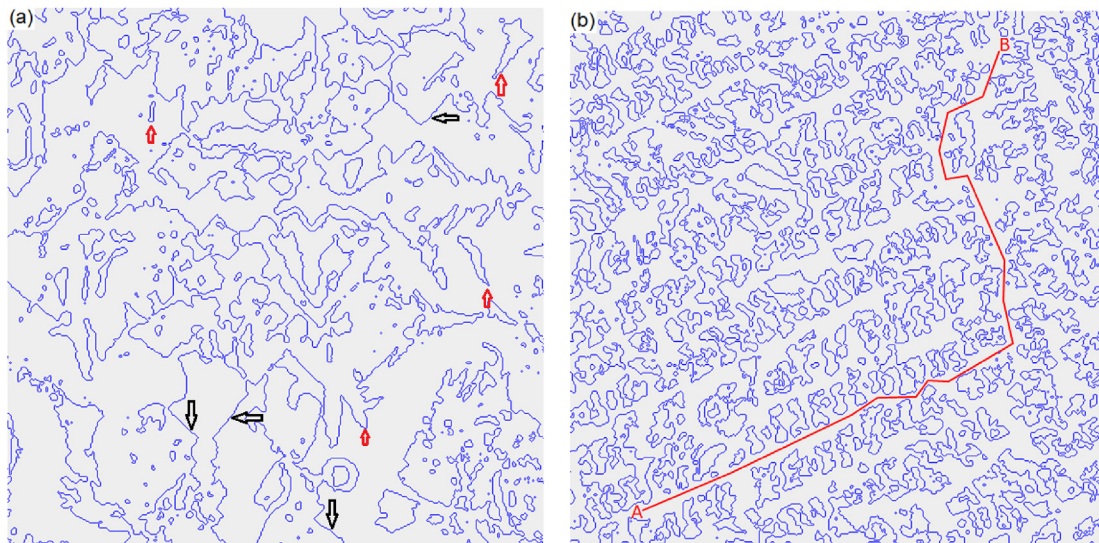


Fig. 7 – The interface between the primary crystals and the eutectic matrix in (a) from a central part in Fig. 3(e) for a reference sample, and (b) from a central part in Fig. 3(f) for a electropulsing treated sample.

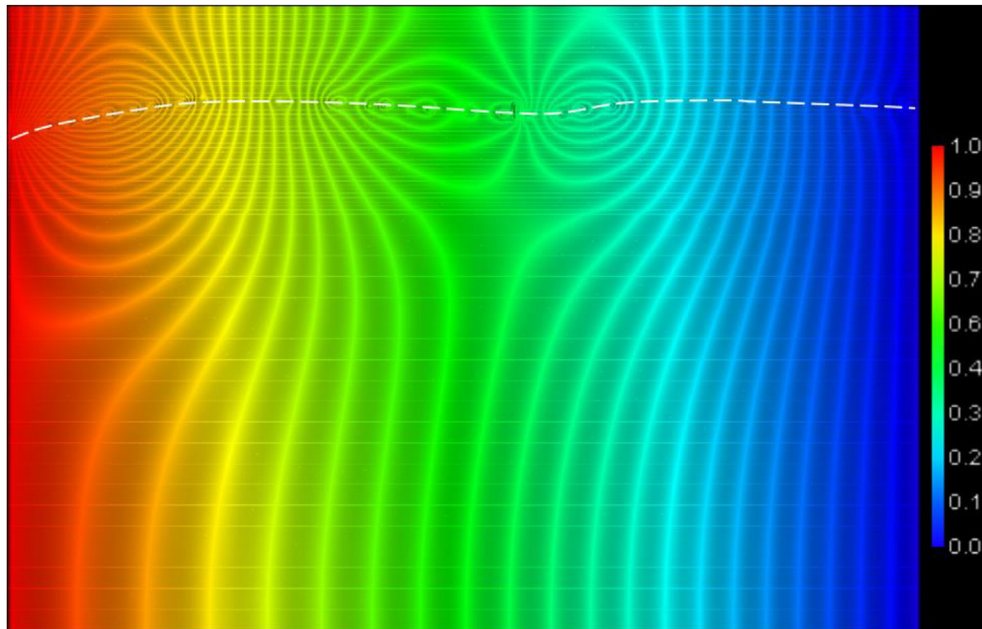


Fig. 8 – Numerical calculation shows the jump of electric potential (vortex) around interface (dashed line) in the mould flux. The legend indicates the electric potential.

The interconnected liquid phase enables the electrical conductivity to maintain a highest possible level. This is because the electricity is conducted by the moving ionic atoms. The higher electrical conductance microstructure has lower electric current free energy [10,17,26]. On the other side, the higher electric conductance state corresponds to a lower viscosity [28]. The lower viscosity state also helps the reduction of pores. Lower viscosity allows melt to fill the cavities effectively which typically result from shrinkage from crystallization. This in turn reduces number of pores.

To understand the electric-current-induced temperature change in the electropulsing treated samples, the temperature rising rate due to Joule heat has been calculated according to the equation $\Delta \dot{T} = j^2 \Delta t \omega / (\sigma c \rho)$, where $j = 2 \times 10^4 \text{ A/m}^2$ is the peak current density, $\Delta t = 60 \mu\text{s}$ is the pulse duration, $\omega = 500 \text{ Hz}$ is the pulse frequency, $\rho = 570 \text{ kg/m}^3$ is the mass density of slag film. σ and c are the electrical conductivity and specific heat, respectively. One chooses the values for liquid CaF_2 for this assessment due to its significant fraction in the mould flux. This gives $\sigma = 4 \Omega^{-1} \text{ cm}^{-1}$ and $c = 854 \text{ J kg}^{-1} \text{ K}^{-1}$. The calculation gives $\Delta \dot{T} = 0.06 \text{ K/s}$, which is much smaller than the average air-cooling rate of 2 K/s demonstrated in Fig. 6. Therefore, the temperature change due to electropulsing treatment is negligible.

This work has not measured the horizontal heat conductivity of the reference and treated samples due to the unavailable facilities. However, literature on the relationship between the microstructure and heat conduction of mould flux is very rich. Both the fraction of the porosity [35] and interface [36] affects thermal conduction. The morphology of the crystallized grains, mostly cuspidine, also adversely affects the lubrication of the mould flux [37,38].

5. Conclusion

This work investigated the effect of electropulsing treatment on the microstructure formation in the solidification of mould flux. Electropulsing has been found to affect the microstructure drastically. Following conclusions have been achieved:

- Electropulsing treatment causes significant reduction of porosity in the solidified materials. This is due to the current-enhanced connectivity of liquid phase during the formation of primary crystal. Liquid phase can compensate the volume shrink during cooling and allows the gas bubbles to escape.
- Electropulsing treatment reduces the interface energy. The presence of the electrical potential difference around the interface causes the polarization of oxide molecules. The electric static interaction reduces the interface energy. The lower interface energy enables the interface to grow into fractal shape. The interfacial perimeter to area ratio is hence increased by over 100%.
- The microstructure in the electropulsing treated samples is drastically different from that solidified without electropulsing. The modified crystal morphology, fraction of interface and porosity can contribute to the horizontal heat conduction and lubrication. Electropulsing is an emerging technology to modify the microstructure of mould flux in order to meet the requirement to cast new advanced steels.

Institutional Review Board Statement

Not applicable.

Informed Consent Statement

Not applicable.

Data Availability Statement

Data is contained within the article.

Funding

The research leading to these results received funding from European Commission's Research Fund for Coal and Steel under Grant Agreement No 847269 and from the Engineering and Physical Sciences Research Council at UK under Grant Agreement No EP/R029598/1.

Declaration of Competing Interest

The authors declare that they have no known competing financial interests or personal relationships that could have appeared to influence the work reported in this paper.

Acknowledgements

The authors are grateful to Karin Hansson-Antonsson and Peter Andersson in Sandvik AB company for provision of oxide powders for making the samples.

REFERENCES

- [1] Mills KC, Fox AB. The role of mould fluxes in continuous casting—so simple yet so complex. *ISIJ Int* 2003;43:1479–86.
- [2] Yang J, Zhu MY. Evolution of compositions and properties of CaO–SiO₂ based mold flux for continuous casting high Mn steel. *ISIJ Int* 2016;56:2191–8.
- [3] Cai ZY, Song B, Li LF, Liu Z, Cui XK. Effect of CeO₂ on heat transfer and crystallization behavior of rare earth alloy steel mould fluxes. *Int. J. Miner. Metall. Mater* 2019;26:565–72.
- [4] Qin R. Critical assessment of the electric effect in electric arc welding. *Metals* 2021;11:1917.
- [5] Misra AK. A novel solidification technique of metals and alloys under the influence of applied potential. *Metall Trans A* 1985;16A:1354–5.
- [6] Misra AK. Misra technique applied to solidification of cast-iron. *Metall Trans A* 1985;17A:358–60.
- [7] Misra AK. Effect of electric potentials on solidification of near eutectic Pb–Sb–Sn alloy. *Mater Lett* 1986;4:176–7.
- [8] Li JM, Li SL, Li J, Lin HT. Modification of solidification structure by pulse electric discharging. *Scripta Metall Mater* 1994;31:1691–4.
- [9] Barnak JP, Sprecher AF, Conrad H. Colony (grain) size reduction in eutectic Pb–Sn castings by electropulsing. *Scripta Metall Mater* 1995;32:879–84.
- [10] Qin RS, Zhou BL. Effect of electric current pulses on grain size in castings. *Int J Non Equilib Process* 1998;11:77–86.
- [11] Zhang XF, Qin RS. Electric current-driven migration of electrically neutral particles in liquids. *Appl Phys Lett* 2014;104:114106.
- [12] Li N, Zhang LM, Zhang R, Yin PF, Wu HJ, Song KK, et al. The role of electric current-associated free energy and forced convection on grain refinement in pure aluminum under electropulsing. *Materials* 2019;12:3846.
- [13] Wang WL, Ying GM, Zeng J, Zhang HH. Effect of electropulsing treatment on solidification behavior of spring steels in a continuous casting mold simulator. *J Iron Steel Res Int* 2020;27:656–64.
- [14] Liao XL, Zhai QJ, Luo J, Chen WJ, Gong YY. Refining mechanism of the electric current pulse on the solidification structure of pure aluminum. *Acta Mater* 2007;55:3103–9.
- [15] Conrad H. Influence of an electric or magnetic field on the liquid–solid transformation in materials and on the microstructure of the solid. *Mater Sci Eng, A* 2000;A287:205–12.
- [16] Takemoto R, Hizubayashi H. Effects of passing electric current on the structural relaxation and crystallization in amorphous alloys. *Mater Sci Eng, A* 1994;A179–A180:275–8.
- [17] Qin RS, Rahnema A, Lu WJ, Zhang XF, Elliott-Bowman B. Electropulsed steels. *Mater Sci Technol* 2014;30:1040–4.
- [18] Riaz S. Effect of electric potential on mould powder behaviour during solidification. *Ironmak Steelmak* 2012;39:409–13.
- [19] Raj R, Cologna M, Francis JSC. Influence of externally imposed and internally generated electrical fields on grain growth, diffusional creep, sintering and related phenomena in ceramics. *J Am Ceram Soc* 2011;94:1941–65.
- [20] Zhao ST, Zhang RP, Chong Y, Li XQ, Abu-Odeh A, Rothchild E, et al. Defect reconfiguration in a Ti–Al alloy via electroplasticity. *Nat Mater* 2021;20:468–72.
- [21] Kim MJ, Yoon SM, Park SW, Jeong HJ, Park JW, Kim KT, et al. Elucidating the origin of electroplasticity in metallic materials. *Appl Mater Today* 2020;21:100874.
- [22] Qin RS, Fan Z. Fractal theory study on morphological dependence of viscosity of semisolid slurries. *Mater Sci Technol* 2021;17:1149–52.
- [23] Zhang GZ, Qin SY, Yan LG, Zhang XF. Superior dehydrogenation performance of Mg-based alloy under electropulsing. *Scripta Mater* 2021;197:113788.
- [24] Gu SP, Wen GH, Ding ZQ, Guo JL, Tang P, Liu Q. Effect of bubbles on crystallization behavior of CaO–SiO₂ based slags. *Metals* 2019;9:193.
- [25] Qin RS. Artificial neural network study of the electrical conductivity of mould flux. *Mater Sci Technol* 2021;37:1476–82.
- [26] Winterhager H, Kammel R, Gad A. Electric conductivity, density and surface tension of fluoride type slag for electrosag remelting method. *Electric Steelmaking* 1974;45:234–52.
- [27] Zhang GH, Zheng WW, Jiao SQ, Chou KC. Influences of Na₂O and K₂O additions on electrical conductivity of CaO–SiO₂–(Al₂O₃) melts. *ISIJ Int* 2017;57:2091–6.
- [28] Qin R. Using electric current to surpass the microstructure breakup limit. *Sci Rep* 2017;7:41451.
- [29] Qin RS. Suppression of the surface roughness and fluctuation frequency by electric Method. *Mater Today Commun* 2021;28:102512.
- [30] Qin R, Bhagurkar A. Effect of pulsating solidification on the surface properties of conductive materials. *Proc. R. Soc. A* 2022;478:20210726.
- [31] Zhang GH, Chou KC. Simple method for estimating the electrical conductivity of oxide melts with optical basicity. *Metall Mater Trans* 2010;41B:131–6.
- [32] Mathur A, Sharma P, Cammarata RC. Negative surface energy — clearing up confusion. *Nat Mater* 2005;4:186.
- [33] Mullins WW, Sekerka RF. Stability of a planar interface during solidification of a dilute binary alloy. *J Appl Phys* 1964;35:444.
- [34] Witten TA, Sander LM. Diffusion-limited aggregation, a kinetic critical phenomenon. *Phys Rev Lett* 1981;47:1400–3.

-
- [35] Hanao M, Kawamoto M, Yamanaka A. Influence of mold flux on initial solidification of hypo-peritectic steel in a continuous casting mold. *ISIJ Int* 2012;52:1310–9.
- [36] Shibata H, Emi T, Waseda Y, Kondo K, Ohta H, Nakajima K. Thermal diffusivities of continuous casting mold fluxes for steel in the glassy and crystalline states. *J Iron Steel Inst Jpn* 1996;82:504–8.
- [37] Cho JW, Blazek K, Frazee M, Yin HB, Park JH, Moon SW. In: Assessment of CaO-Al₂O₃ based mold flux system for high aluminum TRIP casting. 53; 2013. p. 62–70.
- [38] Guo J, Seo MD, Shi CB, Cho JW, Kim SH. Control of crystal morphology for mold flux during high-aluminum AHSS continuous casting process. *Metall Mater Trans* 2016;47B:2211–21.